ECONTECHMOD. AN INTERNATIONAL QUARTERLY JOURNAL – 2018, Vol. 07, No. 1, 87–96

Two-stage scheme for identification of parallel Scott-Blair fractional model of viscoelastic biological materials

Anna Stankiewicz

Department of Technology Fundamentals, University of Life Sciences in Lublin, Poland
e-mail: anna.stankiewicz@up.lublin.pl

Received: February 21, 2018; Accepted: March 01, 2018

Abstract. Fractional calculus considers derivatives and integrals of an arbitrary order. This article focuses on fractional parallel Scott-Blair model of viscoelastic biological materials, which is a generalization of classic Kelvin-Voight model to non-integer order derivatives suggested in the previous paper. The parallel Scott-Blair model admit the closed form of analytical solution in terms of two power functions multiplied by Debye type weight function. To build a parallel Scott-Blair model when only discrete-time measurements of the relaxation modulus are accessible for identification is a basic concern. Based on asymptotic models a two-stage approach is proposed for fitting the measurement data, which means that in the first stage the data are fitted by solving two dependent, but simple, linear least-squares problems in two separate time intervals. Next, at the second stage of the identification procedure the exact parallel Scott-Blair model optimal in the least-squares sense is computed. The log-transformed relaxation modulus data is used in the first stage of identification scheme, while the original relaxation modulus data is applied for the second stage identification. A complete identification procedure is presented. The usability of the method to find the parallel Scott-Blair fractional model of real biological material is demonstrated. The parameters of the parallel Scott-Blair model of a sample of sugar beet root, which very closely approximate the experimental relaxation modulus data, are given.

Key words: fractional calculus, viscoelasticity, relaxation modulus, parallel Scott-Blair fractional model, model identification.

INTRODUCTION

Traditional methods to describe the viscoelastic materials include several spring and dashpot elements to model integer order differential equations in time domain. These classical derivatives can be extended including fractional order derivatives. For a few decades fractional calculus has encountered much success in the mathematical modeling of complex dynamical systems. It has been proved, in particular, that fractional calculus constitutes a valuable mathematical tool to handle viscoelastic aspects of systems and materials mechanics [4,7,8,14]. Since both the Maxwell element and the Kelvin-Voigt element of Debye type decay do not fully characterize the true viscoelastic behavior of some materials, rheology theorists were early to realize the importance of incorporating fractional-calculus techniques. The first papers which adopted and utilized fractional order dynamics go back to the 1970s [13], when elementary fractional Scott-Blair element was introduced. By replacing the springs and dashpots of the classical viscoelastic models with the Scott-Blair elementary fractional elements, several fractional models, including the fractional Maxwell, fractional Voigt and fractional Kelvin models, have been proposed [6,10,12]. An overview of fractional viscoelastic models is presented in [9]. In the previous paper a parallel Scott-Blair model was suggested connecting in parallel two Scott-Blair models with additional multiplicative weight functions. The proposed model takes into account the change of the rheological properties of biological materials during the relaxation process.

The aim of the paper is to develop a complete procedure for the parallel Scott-Blair model identification based on discrete time relaxation modulus data from stress relaxation test. If the classic mean sum of squares is taken as a measure of the model accuracy, the resulting task of fitting data to the model is a very difficult problem of nonlinear optimization, numerically difficult and often ill-conditioned both due to the exponential weight function and to the power-type elementary fractional components. Here, to reduce these inconveniences this task is solved in two-stages. Based on the asymptotic properties of the parallel Scott-Blair model for small and large arguments the approximate formulas are given, which state the basis for model identification. The approximate asymptotic models are composed of only two parameters. By applying the logarithmic transformation of the power

type asymptotic models and experimental data, the original nonlinear identification tasks are reduced to linear least-squares problems. As a result, at the first stage two Scott-Blair models are determined by applying the linear least-squares for log transformed models and experimental data in two separate time intervals. To develop the identification routine in the first stage we use the known result concerning the linear least-square method and we provide the expressions for the estimators of the optimal models parameters. In the second stage the optimal parameter of Debye decay type weight function is chosen in order to guarantee the best fit of experimental data. The original complete set of measurement data is used here. A complete algorithm is proposed for the parallel Scott-Blair fractional model identification based on the discrete time stress relaxation experimental data.

Research studies conducted during the past few decades have proved that viscoelastic models are also an important tool for studying the behavior of biological materials, which present a behavior that implies dissipation and storage of mechanical energy [11,13,19,21]: wood, fruits, vegetables, animal tissues, etc. The effectiveness of the parallel Scott-Blair model and the identification routine proposed is demonstrated for real biological material and compared with the classical four parameter Maxwell model approximation.

PARALLEL SCOTT-BLAIR MODEL

We consider a linear viscoelastic material subjected to small deformations and we restrict our attention to the one-axial case assuming that the viscoelastic material is quiescent for all times prior to starting instant, that we assume as $t = 0$. In the previous paper a new viscoelastic model – parallel Scott-Blair model – was proposed as a weighted parallel connection (see Fig. 1b) of two Scott-Blair elementary fractional elements (Fig. 1a) described by the fractional differential equations:

$$\sigma_1(t) = E\tau^{\alpha}\frac{d^{\alpha}\varepsilon(t)}{dt^{\alpha}},$$

$$\sigma_2(t) = E\tau^{\beta}\frac{d^{\beta}\varepsilon(t)}{dt^{\beta}},$$

such that, the linear time-dependent relaxation modulus $G(t)$ is described by the function:

$$G(t) = \frac{E}{\Gamma(1-\beta)}\left(\frac{t}{\tau}\right)^{-\beta}\varphi(t) + \frac{E}{\Gamma(1-\alpha)}\left(\frac{t}{\tau}\right)^{-\alpha}\left(1-\varphi(t)\right). \quad (1)$$

The modulus $G(t)$ is the stress, which is induced in the viscoelastic material when the unit-step strain $\varepsilon(t)$ is imposed. Here $\sigma_1(t)$ and $\sigma_2(t)$ denotes the stresses, $\varepsilon(t)$ is the stain, E and τ are the elastic modulus and relaxation time, α and β are non-integer positive order of fractional derivatives of the strain $\varepsilon(t)$. Here, $\frac{d^{\beta}}{dt^{\beta}} = D_t^{\beta}$ means the derivative operator in the sense of the Caputo's fractional derivative of a function $f(x)$ of non-integer order β with respect to variable t and with starting point at $t = 0$, which is defined by [8]:

$$D_t^{\beta}f(t) = \frac{1}{\Gamma(n-\beta)}\int_0^t (t-1)^{n-\beta-1}\frac{d^n}{dt^n}f(t)dt,$$

where $n-1 < \beta < n$, and $\Gamma(x)$ is Euler's gamma function defined by the integral:

$$\Gamma(x) = \int_0^{\infty} t^{x-1}e^{-t}dt. \quad (2)$$

The exponential decay weight function is assumed:

$$\varphi(t) = e^{-\gamma t}, \quad (3)$$

of exponential decay represented by the parameter $\gamma > 0$, thus the relaxation modulus (1) has the following exact form:

$$G(t) = \frac{E}{\Gamma(1-\beta)}\left(\frac{t}{\tau}\right)^{-\beta}e^{-\gamma t} + \frac{E}{\Gamma(1-\alpha)}\left(\frac{t}{\tau}\right)^{-\alpha}(1-e^{-\gamma t}). \quad (4)$$

The model is composed by analogy to the classic Kelvin-Voight by the parallel arrangement of two fractional Scott-Blair elements (E, τ, α) and (E, τ, β), i.e. by replacing the standard purely elastic spring and purely viscous dashpot of the classical Kelvin-Voight model by two Scott–Blair elements, with additional multiplicative elements of product operation represented by means of the weight function $\varphi(t)$. In Fig. 1b the multiplication operations in (1) are symbolically marked by the product blocks in two parallel branches. Without any loss of generality we assume that $1 > \alpha \geq 0$ and $1 > \beta \geq 0$. We also allow one, but not both, of the α and β values to be zero.

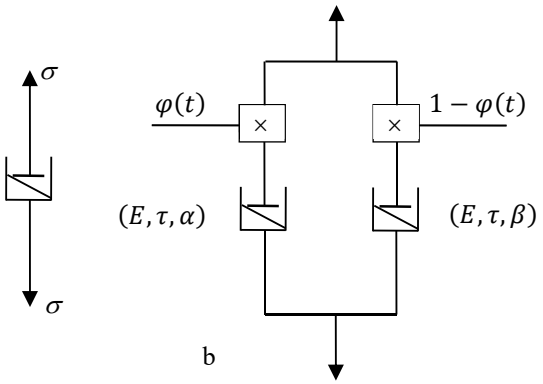

Fig. 1. Fractional Scott-Blair element (a) followed by the parallel Scott-Blair fractional model (b)

ASYMPTOTIC APPROXIMATIONS

In the interpretation of asymptotic behavior of the parallel Scott-Blair model a fundamental role is played by the asymptotic properties of the weight function $\varphi(t)$ (3). Since for small t, in particular for $\gamma t \cong 0$, we have $\varphi(t) = e^{-\gamma t} \cong 1$, whence $1 - \varphi(t) \cong 0$ and asymptotic approximation results:

$$G(t) \cong G_1(t) = \frac{E}{\Gamma(1-\alpha)}\left(\frac{t}{\tau}\right)^{-\alpha}, \tag{5}$$

here $\cong$ means 'approximately equal'. By the obvious asymptotic property $\varphi(t) \cong 0$, which holds for $\gamma t \to \infty$, i.e. for large times, based on (4) we obtain the next asymptotic approximation of the parallel Scott-Blair model in the form:

$$G(t) \cong G_2(t) = \frac{E}{\Gamma(1-\beta)}\left(\frac{t}{\tau}\right)^{-\beta}. \tag{6}$$

Thus, both for short and for large times, relaxation modulus (4) decreases almost according to the time-power elementary fractional element. The approximate models (5), (6) and the exact parallel Scott-Blair model are summarized in Fig. 2, where logarithmic scale is used both for relaxation modulus and time. Here, the asymptotic models (5), (6), whose graph is a straight line are linear functions, which slope coefficients uniquely determine as the fractional derivatives orders – α for small times and β for large times, respectively.

Note, that both for small and for large times the fractional Scott-Blair model is appropriate to describe the relaxation process, but the orders of the two models (5) and (6) are different. The authors, in particular Bohdziewicz [1-3], point out that during the relaxation process the mechanical properties of the biological material changes. This is an interesting property of such materials. Thus the two models (5) and (6) with non-identical orders β and α are the mathematical meaning of such property. The Scott-Blair model $G_1(t)$ takes into account small times, while $G_2(t)$ model takes into account the long term response. The non-stationary character of the relaxation process is taken into account by an appropriate choice of parameter γ.

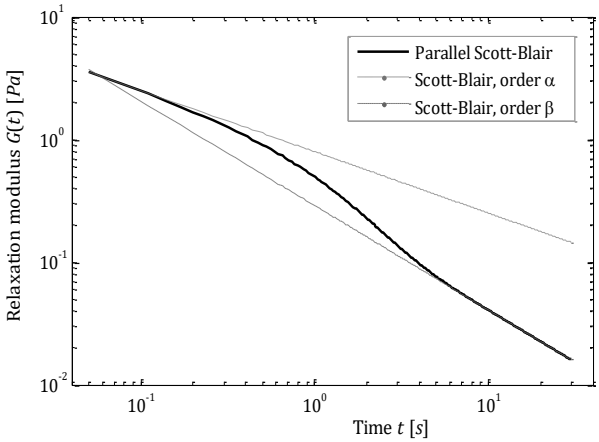

Fig. 2. Relaxation modulus of parallel Scott-Blair model and asymptotic Scott-Blair models for parameters: $\alpha = 0.5, \beta = 0.85, E = 1\ [Pa], \tau = 2\ [s], \gamma = 0.9$

IDENTIFICATION

By assumption, the exact mathematical description of the relaxation modulus $G(t)$ is completely unknown, but the value of $G(t)$ can be measured with a certain accuracy for any given value of the time t. A classical manner of studying viscoelasticity is by two-phase stress relaxation test, where the strain increases during the loading time interval until a predetermined strain ε_0 is reached at a given ramp-time, after which the strain ε_0 is maintained constant at that value [5,15,16].

Suppose a certain stress relaxation test performed on the specimen of the material under investigation resulted in a set of measurements of the relaxation modulus $\bar{G}(t_i)$ at the sampling instants $t_i > 0, i = 1, \dots, N$. For computational methods of relaxation modulus determination see, for example [15,16].

In general, identification consists of the selecting, within the given class of models, of such a model, which ensures the best fit to the measurement results. Fitting data to the original parallel Scott-Blair model (4) is a nonlinear optimization problem, numerically difficult and often ill-conditioned mainly due to the exponential form of the weight function and power form of the Scott-Blair model responses, in which the unknown model parameters α and β are in the exponent, but also due to the multiplicative form of (4) components.

Here, a two-stage approach will be used, in which the linear least-squares identification routine will be applied to estimate parallel Scott-Blair model parameters based on the logarithmic transformation of the experimental data and equations (5), (6) which, respectively, yields:

$$log\, G(t) \cong k_1 - \alpha log t,$$
$$log\, G(t) \cong k_2 - \beta log t,$$

where:

$$k_1 = log\left[\frac{E\tau^{\alpha}}{\Gamma(1-\alpha)}\right], \tag{7}$$

$$k_2 = log\left[\frac{E\tau^{\beta}}{\Gamma(1-\beta)}\right], \tag{8}$$

are introduced for brevity. Denoting $\chi(t) = log\, G(t)$ and introducing the new independent variable $\vartheta = logt$, equivalent linear models are obtained (the sign $\cong$ is neglected for simplicity):

$$\chi(t) = k_1 - \alpha\vartheta, \tag{9}$$

$$\chi(t) = k_2 - \beta\vartheta. \tag{10}$$

Now, in the set of experimental data $\{(\bar{G}(t_i), t_i)\}_{i=1}^{N}$, or equivalently in the set $\{(\chi_i, \vartheta_i)\}_{i=1}^{N}$, where:

$$\chi_i = log\,\bar{G}(t_i) \text{ and } \vartheta_i = log\, t_i, \tag{11}$$

are log-transformed 'measurement' data, two separable subsets $\{(\chi_i, \vartheta_i)\}_{i=1}^{n_1}$ and $\{(\chi_i, \vartheta_i)\}_{i=n_2}^{N}$ must be determined such that $n_1 < n_2$, probably $n_1 \ll n_2$. The subsets $\mathcal{N}_1 = \{1, \dots, n_1\}$ and $\mathcal{N}_2 = \{n_2, \dots, N\}$ of respective indices are chosen during the recurrent identification scheme. It is clear that the union of the sets $\mathcal{N}_1 \cup \mathcal{N}_2$ does not create the set $\mathcal{N} = \{1, \dots, N\}$. Now, classic linear least-squares method can be applied to find optimal approximate models.

As a measure of the model (9) accuracy the mean sum of squares is taken:

$$Q_1(k_1, \alpha, n_1) = \frac{1}{n_1}\sum_{i=1}^{n_1}[\chi_i - k_1 + \alpha\vartheta_i]^2, \tag{12}$$

the respective identification index for the second set of experimental data and log-linearized model (10) is:

$$Q_2(k_2, \beta, n_2) = \frac{1}{N-n_2+1}\sum_{i=n_2}^{N}[\chi_i - k_2 + \beta\vartheta_i]^2. \tag{13}$$

Therefore, the least-squares identification of the log-linearized models consists of determining the model parameters minimizing the indices (12), (13) by solving the following standard optimization problems:

$$Q_1\left(\hat{k}_{1,n_1}, \hat{\alpha}_{n_1}, n_1\right) = min_{(k_1,\alpha)\in R^2}\, Q_1(k_1, \alpha, , n_1), \tag{14}$$

$$Q_2\left(\hat{k}_{2,n_2}, \hat{\beta}_{n_2}, n_2\right) = min_{(k_2,\beta)\in R^2}\, Q_2(k_2, \beta, n_2). \tag{15}$$

Based on the well-known results concerning the linear least-squares problem solution, it can be shown that the solutions to (14), (15) tasks exist and are unique whenever the sampling instants are such that $0 < t_1 < t_2 < \dots < t_N$. The model parameters optimal in the sense of (14) admit the closed form of analytical solution in terms of the log-transformed data (11) and they are given by the known formulas:

$$\hat{\alpha}_{n_1} = \frac{\frac{1}{n_1}\sum_{i=1}^{n_1}\chi_i\sum_{i=1}^{n_1}\vartheta_i - \sum_{i=1}^{n_1}\chi_i\vartheta_i}{\sum_{i=1}^{n_1}[\vartheta_i]^2 - \frac{1}{n_1}\left[\sum_{i=1}^{n_1}\vartheta_i\right]^2}, \tag{16}$$

$$\hat{k}_{1,n_1} = \frac{1}{n_1}\sum_{i=1}^{n_1}\chi_i + \frac{1}{n_1}\sum_{i=1}^{n_1}\vartheta_i\,\hat{\alpha}_{n_1}. \tag{17}$$

The formulas for model (10) optimal parameters are analogous, i.e. they are given by:

$$\hat{\beta}_{n_2} = \frac{\sum_{i=n_2}^{N}\chi_i\sum_{i=n_2}^{N}\vartheta_i - (N-n_2+1)\sum_{i=n_2}^{N}\chi_i\vartheta_i}{(N-n_2+1)\sum_{i=n_2}^{N}x_ix_i - \sum_{i=n_2}^{N}x_i\sum_{i=n_2}^{N}x_i}, \tag{18}$$

$$\hat{k}_{2,n_2} = \frac{1}{N-n_2+1}\sum_{i=n_2}^{N}\chi_i + \frac{1}{N-n_2+1}\hat{\beta}_{n_2}\sum_{i=n_2}^{N}\vartheta_i. \tag{19}$$

According to definitions (7) and (8) the positivity constraint can be neglected for k_1 and k_2 in (14), (15) optimization tasks. However, both α as well as β must be positive. Based on the Chebyshev equality the following result can be obtained; the proof is omitted here due to space limitations.

Property 1. The optimal parameters $\hat{\alpha}_{n_1}$ and $\hat{\beta}_{n_2}$ are positive, if and only if, the following conditions are valid:

$$\sum_{i=1}^{n_1}\sum_{j=i+1}^{n_1} log\frac{\bar{G}(t_j)}{\bar{G}(t_i)}\; log\frac{t_i}{t_j} > 0,$$

$$\sum_{i=n_2}^{N}\sum_{j=i+1}^{N} log\frac{\bar{G}(t_j)}{\bar{G}(t_i)}\; log\frac{t_i}{t_j} > 0,$$

for tasks (14) and (15), respectively.

Note, that the models (9) and (10) include two unknown parameters (k_1, α) and (k_2, β). In view of (8) and (7) the above pairs of parameters are not independent. Therefore, from (8) and (7) for the optimal parameters we have:

$$\hat{\tau}_{n_1,n_2} = \left[\frac{\Gamma(1-\hat{\beta}_{n_2})}{\Gamma(1-\hat{\alpha}_{n_1})}10^{\hat{k}_{2,n_2}-\hat{k}_{1,n_1}}\right]^{\frac{1}{\hat{\beta}_{n_2}-\hat{\alpha}_{n_1}}}, \tag{20}$$

which, in view of (8), next yields:

$$\hat{E}_{n_1,n_2} = 10^{\hat{k}_{2,n_2}}\frac{\Gamma(1-\hat{\beta}_{n_2})}{\tau^{\hat{\beta}_{n_2}}}. \tag{21}$$

Of course, we can find the sum-square model errors $Q_1(k_1, \alpha, n_1)$ (12) and $Q_2(k_2, \beta, n_2)$ (13) over some finite time intervals, but what interval, i.e., what measurement

points, should we choose? To select an appropriate subset of measurement points we adopt the simple procedure based on the conditions $e^{-\gamma t} \cong 1$ and $e^{-\gamma t} \cong 0$, which implies the asymptotic approximations $G_1(t)$ and $G_2(t)$, respectively. Taking into account the course of the weight function $\varphi(t) = e^{-\gamma t}$ we assume the following conditions:

$$t_{n_1}\gamma \leq 0.051293, \tag{22}$$

and

$$t_{n_2}\gamma \geq 2.995732, \tag{23}$$

to guarantee $\varphi(t) \geq 0.95$ for any $t \leq t_{n_1}$ and $\varphi(t) \leq 0.05$ for any $t \geq t_{n_2}$.

Now the parameter γ of the weight function should be found. The search of the model parameter γ is based on the classic least-squares fitting of measurement data. In order to find optimal γ all the measurements $\{(\bar{G}(t_i), t_i)\}_{i=1}^{N}$ will be used. The mean sum of squares related to the original model (4) is applied as measure of the model (4) accuracy:

$$Q(\gamma) = \frac{1}{N}\sum_{i=1}^{N}[\bar{G}(t_i) - G(t_i, \gamma)]^2, \tag{24}$$

where the notation $G(t_i, \gamma)$ is introduced for the model $G(t)$ in order to highlight the dependence of the model parameter γ. The respective optimal identification task follows:

$$Q(\hat{\gamma}) = min_{\gamma>0}\, Q(\gamma). \tag{25}$$

Simple sufficient condition for the existence of the optimal parameter $\hat{\gamma}$ is given in the following result, the proof is omitted as before.

Property 2. Assume that the relaxation modulus measurements $\bar{G}(t_i)$ are bounded, $i = 1,2, \dots, N$. If the following conditions are satisfied:

$$\sum_{i=1}^{N}[\bar{G}(t_i) - G_1(t_i)]\,[G_1(t_i) - G_2(t_i)]t_i < 0, \tag{26}$$

and

$$[\bar{G}(t_1) - G_2(t_1)][G_1(t_1) - G_2(t_1)]t_1 > 0, \tag{27}$$

then there exists the solution to the optimal identification task (25).

Note, that (26) and (27) are *a posteriori* conditions, since they cannot be checked, earlier than after the experiment is performed. Note also, that since for $\gamma < 0$ the exponential functions $e^{-\gamma t_i}$ grow to infinity as $\gamma \to -\infty$, in result $Q(\gamma) \to \infty$, the constraint $\gamma > 0$ can be indeed omitted in (25) task. The numerical experiments showed that the function $Q(\gamma)$ usually has unique minimum. The exemplary course of $Q(\gamma)$ are plotted in Fig. 12 below.

IDENTIFICATION SCHEME

Taking into account the above, the calculation of the approximate values of parallel Scott-Blair model parameters involves the following steps.

1. Perform the stress relaxation test, record and store the relaxation modulus measurements $\bar{G}(t_i)$ corresponding to the chosen sampling instants $t_i > 0$, $i = 1, \dots, N$.
2. Determine the set $\{(\chi_i, \vartheta_i)\}_{i=1}^{N}$ of log-transformed measurement data (11).
3. Based on the course of log-log plot of the measurement data, select in the set of measurements two separable subsets choosing n_1 and n_2, $n_1 < n_2$.
4. Compute the estimates $(\hat{\alpha}_{n_1}, \hat{k}_{1,n_1})$ and $(\hat{\beta}_{n_2}, \hat{k}_{2,n_2})$ according to formulas (16)-(19).
5. In order to ascertain if the models with parameters $(\hat{\alpha}_{n_1}, \hat{k}_{1,n_1})$ and $(\hat{\beta}_{n_2}, \hat{k}_{2,n_2})$ are a satisfactory approximation of measurement data in time intervals $(0, t_{n_1}]$ and $[t_{n_2}, t_N]$ compute the optimal identification indices and examine if $Q_1(\hat{k}_{1,n_1}, \hat{\alpha}_{n_1}, n_1) \leq \delta$ and $Q_2(\hat{k}_{2,n_2}, \hat{\beta}_{n_2}, n_2) \leq \delta$ for δ, a preselected small positive error. If not, change n_1 and/or n_2 and go to Step 4. Otherwise, go to Step 6.
6. Compute the estimates of the relaxation time $\hat{\tau}_{n_1,n_2}$ and elastic modulus $\hat{E}_{n_1,n_2}$ using (20) and (21) formulas.
7. Find weight function parameter $\hat{\gamma}_{n_1,n_2}$ solving the second stage optimization task (25).
8. In order to ascertain if the asymptotic Scott-Blair models (10), (12) with optimal parameters $(\hat{E}_{n_1,n_2}, \hat{\tau}_{n_1,n_2}, \hat{\alpha}_{n_1})$ and $(\hat{E}_{n_1,n_2}, \hat{\tau}_{n_1,n_2}, \hat{\beta}_{n_2})$ are a satisfactory approximation of the original parallel Scott-Blair model examine if:

$$t_{n_1}\hat{\gamma}_{n_1,n_2} \leq 0.051293, \tag{28}$$

$$t_{n_2}\hat{\gamma}_{n_1,n_2} \geq 2.995732. \tag{29}$$

If both the above conditions are satisfied, stop the procedure taking $(\hat{E}_{n_1,n_2}, \hat{\tau}_{n_1,n_2}, \hat{\alpha}_{n_1}, \hat{\beta}_{n_2}, \hat{\gamma}_{n_1,n_2}) = (\hat{E}, \hat{\tau}, \hat{\alpha}, \hat{\beta}, \hat{\gamma})$ as the parallel Scott-Blair model parameters. If not, change n_1 and/or n_2 and repeat Steps 4-8.

Figure 3 illustrates this procedure. The stopping rules from Step 5 guarantee the good quality of the log-linearized models in the chosen time intervals and corre-

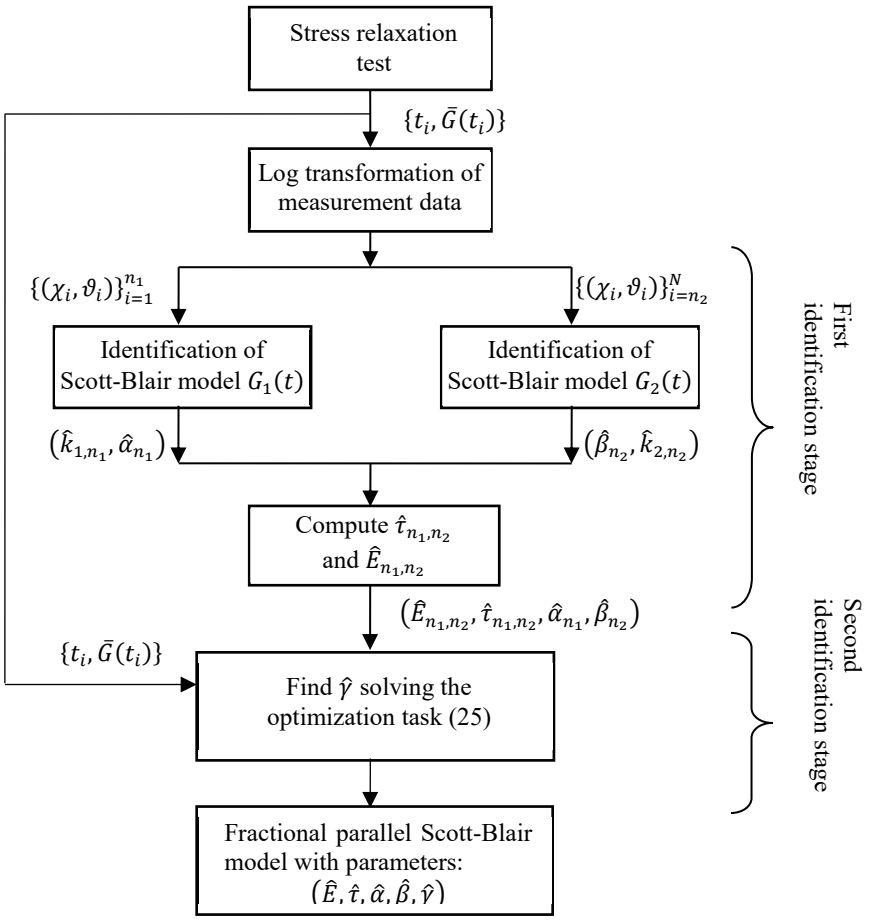

Fig. 3. Two-stage two-interval scheme for parallel Scott-Blair model identification

spond with those commonly used in the optimal identification techniques. The conditions (28), (29) are imposed to guarantee the applicability of Scott-Blair models (10), (12) to approximate the original parallel Scott-Blair model. Both the pairs of conditions must be satisfied simultaneously in order to guarantee good quality of the resulted model. While $\hat{\alpha}_{n_1}$ and $\hat{\beta}_{n_2}$ are determined independently in appropriate time intervals, the relaxation time $\hat{\tau}_{n_1,n_2}$ and the modulus $\hat{E}_{n_1,n_2}$ depend on the identification results in both time intervals, simultaneously. Note also, that (28) and (29) are *a posteriori* conditions, since the applicability of the identification procedure cannot be checked, earlier than after the experiment and the computations are performed.

The next example shows, how the identification scheme can be used for identification of parallel Scott-Blair model of real material.

PARALLEL SCOTT-BLAIR MODEL FOR A SAMPLE OF SUGAR BEET ROOT

In this section we find the parallel Scott-Blair models describing mechanical properties of the root of sugar beet Janus variety and compare them to the optimal classic four-parameter Maxwell models. Cylindrical samples of 20 mm diameter and height were obtained from the root of sugar beet [15,17,18]. During the two-phase stress relaxation test, in the first initial phase the strain was imposed instantaneously, the sample was preconditioned at the $1.5\ m \cdot s^{-1}$ strain rate to the maximum strain for sample numbered as 3. Next, during the second phase at constant strain the corresponding time-varying force induced in the specimen was recorded during the time period $(0{,}100)$ seconds in $N = 1160$ measurement points. The experiment was performed in the state of uniaxial deformation; i.e. the specimen examined underwent deformation in steel cylinder (for details see, for example, [15]). The modeling of mechanical properties of this material in linear-viscoelastic regime is justified by the research results presented in a lot of works, for example [1,15,18]. For the initial filtering of the stress measurement data the Savitzky-Golay method was used. Next, the respective relaxation modulus measurements were computed using fast trapezoidal method of approximate relaxation modulus identification presented in [16]. The proposed identification scheme is implemented in Matlab code. The Matlab standard function `fminbnd` is used for numerical implementation of the second stage optimization task.

Based on the log-log plot of the experiment results for exemplary sample 3 (see Fig. 5), the time intervals deter-

mined by $t_{n_1} = 0.008\ [s]$ and $t_{n_2} = 10\ [s]$ were chosen as well as the estimates of Scott-Blair models parameters, and next the estimates of the relaxation time and elastic modulus were computed. Next, the optimal parameter $\hat{\gamma}_{n_1,n_2}$ was found in the second stage computations, and the resulting parallel Scott-Blair model (4) was obtained. The inaccurate fit of the model $G(t)$ (4) to the experimental data is illustrated in Fig. 4. The relaxation modulus of the classic four-parameter optimal in the least-square sense Maxwell model:

$$G_M(t) = E_1 e^{-v_1 t} + E_2 e^{-v_2 t}, \tag{30}$$

where: $E_1 = 10.9552\ [MPa]$, $E_2 = 2.43487\ [MPa]$ and $v_1 = 0.001156\ [s^{-1}]$, $v_2 = 3.59744\ [s^{-1}]$ represent the elastic modulus and relaxation frequencies, respectively, are also depicted in Fig. 4. This does not accord with observation of real relaxation stress experiment, so the Maxwell model is inappropriate for their description. Here, the quality of Maxwell and parallel Scott-Blair models are comparable. The results are also summarized in the first raw of Table 1, where the model parameters, the times t_{n_1}, t_{n_2} and the factors $t_{n_1}\hat{\gamma}_{n_1,n_2}$ and $t_{n_2}\hat{\gamma}_{n_1,n_2}$ are given. Also, the value of the empirical mean square model error:

$$ERR = \frac{1}{N}\sum_{i=1}^{N}[\bar{G}(t_i) - G(t_i)]^2 = Q\left(\hat{\gamma}_{n_1,n_2}\right)$$

is included in this table. The model errors are not big (see Table 1), but from Fig. 4 it can be seen that the accuracy of the approximation is insufficient, especially in small times region.

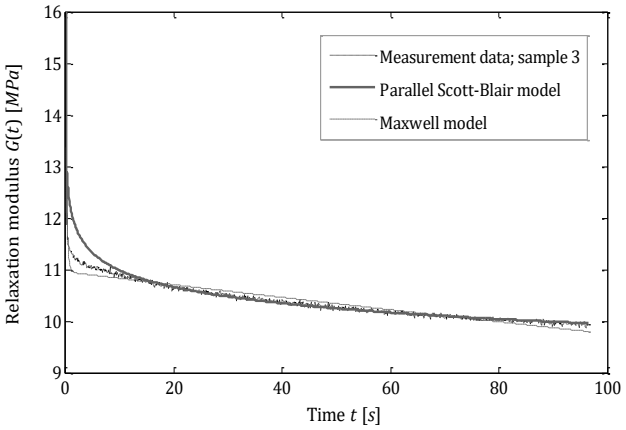

Fig. 4. The inaccurate fit of the parallel Scott-Blair model to experimental data; number of time internals $Nr = 1$

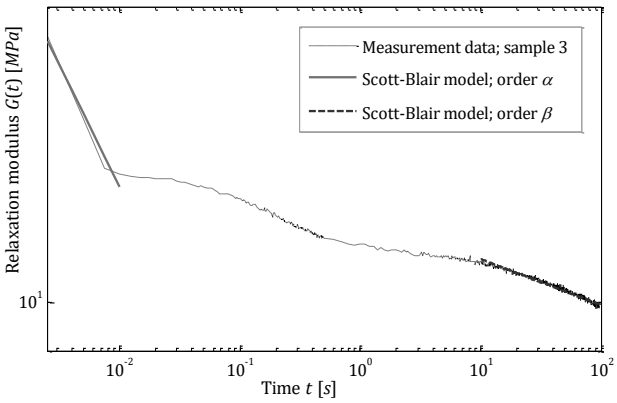

Fig. 5. The log-log plot of elementary Scott-Blair approximate models $G_1(t)$ and $G_2(t)$ for small and large times, respectively; $Nr = 1$

Note, that while the applicability condition (29) for large times is satisfied (the good fit of model $G_2(t)$ for large times is confirmed both in Figure 4 and 5), the second applicability condition (28) is not satisfied for the first attempt ($Nr = 1$) to choose the appropriate time interval $(0, t_{n_1}]$. Thus, $t_{n_1} = 0.06\ [s]$ is assumed, which results in the substantial decrease of the $\hat{\gamma}_{n_1,n_2}$ parameter and yields two-fold decrease in value of the factor $t_{n_1}\hat{\gamma}_{n_1,n_2}$ and sevenfold decrease in model error ERR value. The courses of relaxation modulus (4) and (30) are plotted in Fig. 6, the respective approximate models $G_1(t)$ and $G_2(t)$ are depicted in Fig. 7, the model parameters are given in Table 1 ($Nr = 2$), as above.

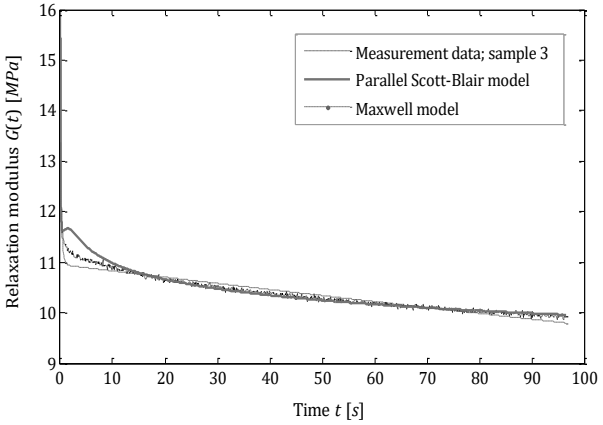

Fig. 6. The time course of parallel Scott-Blair and Maxwell models and the experimental data; $Nr = 2$

Table 1. The results of the parallel Scott-Blair model identification; *Nr* – number of time internals chosen in numerical identification procedure

Nr	$t_{n_1}[s]$	$t_{n_2}[s]$	$\hat{\alpha}_{n_2}$	$\hat{\beta}_{n_1}$	$\hat{\tau}_{n_1,n_2}\ [s]$	$\hat{E}_{n_1,n_2}\ [MPa]$	$\hat{\gamma}_{n_1,n_2}$	ERR	$t_{n_1}\hat{\gamma}_{n_1,n_2}$	$t_{n_2}\hat{\gamma}_{n_1,n_2}$
1	0.008	10	0.2267	0.0432	0.0106	15.1650	20.4612	0,141844	0.164	204.612
2	0.06	10	0.0680	0.0432	0.0025	16.1561	1.3367	0,020822	0.080202	13.367
3	0.1	10	0.0548	0.0432	1.538e-4	18.212	0.3548	0,011202	0.03548	3.548
4	0.5	10	0.0493	0.0432	9.928e-7	22.6480	0.2402	0,011529	0.1201	2.402

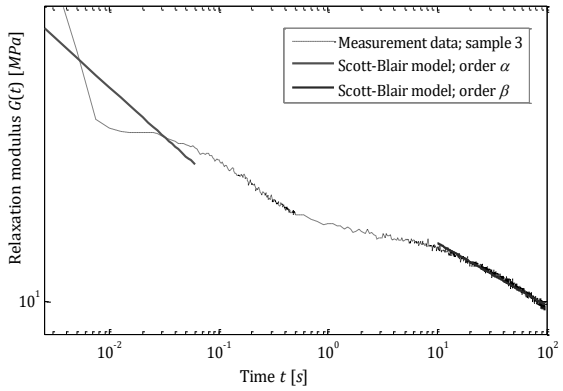

Fig. 7. The log-log plot of elementary Scott-Blair approximate models $G_1(t)$ and $G_2(t)$; $Nr = 2$

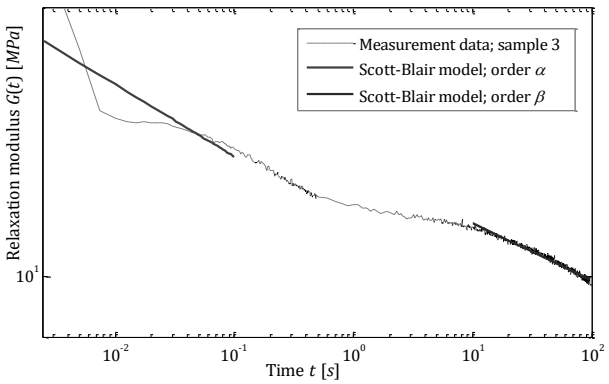

Fig. 9. The log-log plot of Scott-Blair approximate models $G_1(t)$ and $G_2(t)$; $Nr = 3$

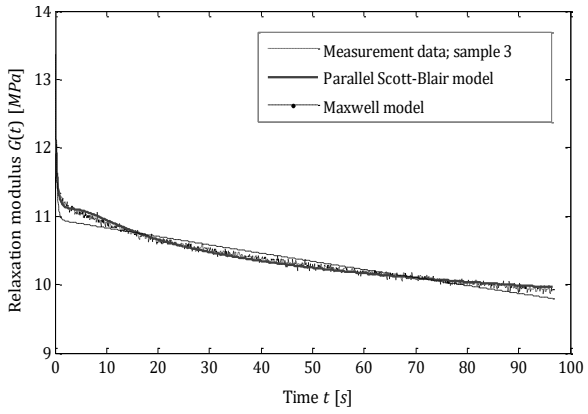

Fig. 8. The time course of the parallel Scott-Blair and Maxwell models and the experimental data; $Nr = 3$

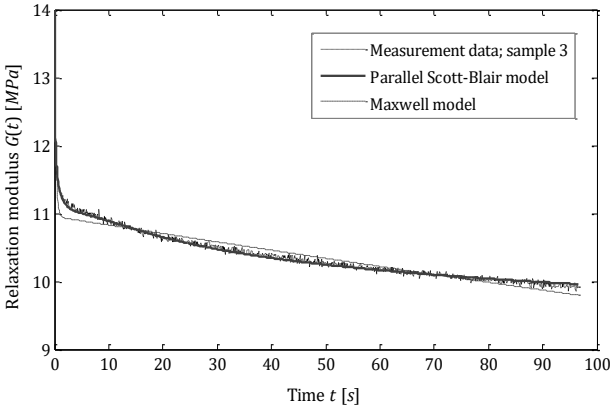

Fig. 10. The time course of parallel Scott-Blair and Maxwell models and the experimental data; $Nr = 4$

This abrupt character of the behavior of parallel Scott-Blair model from Fig. 6 for small times motivated us to reinvestigate the initial time interval to $(0,1]$ with the condition $e^{t_{n_1}\hat{\gamma}_{n_1,n_2}} \cong 0$ in mind. As a result, the model depicted in Fig. 8 was obtained. The respective model and identification process data are summarized for $Nr = 3$ in Table 1. Now, both conditions (28) and (29) of the asymptotic models applicability are satisfied. For $Nr = 3$ choice of the first time interval, essentially better fit to the measurement data is obtained (see also the respective value of the model error ERR in Table 1), but the model $G(t)$ is still not monotonically decreasing (see Fig 8). Thus $t_{n_1} = 0.5\,[s]$ is taken in next step $Nr = 4$ and the parallel Scott-Blair model plotted in Fig. 10 is determined.

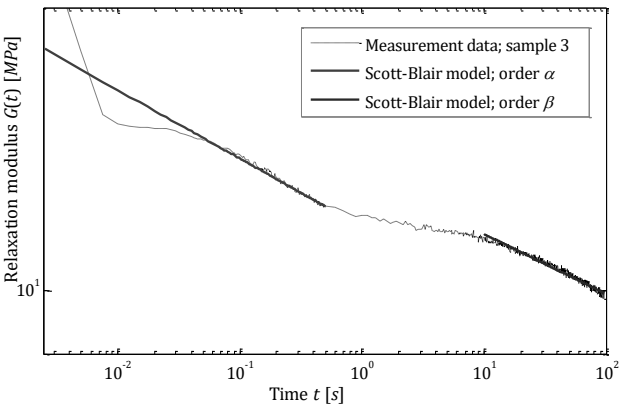

Fig. 11. The log-log plot of Scott-Blair approximate models $G_1(t)$ and $G_2(t)$; $Nr = 4$

Note, that the drawing from Fig. 10 indicates almost perfect model fit to experimental data. In Fig. 12 two exemplary courses of the index $Q(\gamma)$ (24) are demonstrated.

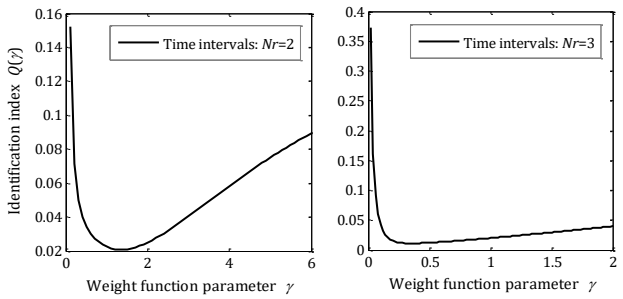

Fig. 12. Two-stage identification index $Q(\gamma)$ (24) as a function of γ

FINAL REMARKS

This paper shows, that the Parallel Scott-Blair model can be fully determined in two stages using only the standard least-squares and log-linearized least-squares techniques. It is also shown herein that the fractional parallel Scott-Blair model can be used to describe the viscoelastic mechanical properties of biological materials.

Mathematical modeling of biological materials is crucial for the design of various applications in the agriculture and food industry [11,18,20,22]. This paper is geared towards the applications of fractional order models in the rheology of biological materials. As such, viscoelastic model design should not be restricted to narrow integer-order derivatives domain.

REFERENCES

1. **Bohdziewicz J. 2007.** Modelowanie przebiegu odkształceń tkanek parenchymy warzyw w warunkach quasi-statycznych zmian obciążeń. Wyd. Uniwersytetu Przyrodniczego, Wrocław.
2. **Bohdziewicz J., Czachor G. 2016.** The rheological properties of redcurrant and highbush blueberry berries. Agricultural Engineering, Vol. 20, No. 2, 15-22.
3. **Bohdziewicz J., Czachor G. Grzemski P. 2013.** Anisotropy of mechanical properties of mushrooms (agaricus bisporus (j.e. lange) imbach). Agricultural Engineering, Vol. 4(148), No.2, 15-23.
4. **Cai W., Chen W., Xu W. 2016.** Characterizing the creep of viscoelastic materials by fractal derivative models. International Journal of Non-Linear Mechanics, Vol. 87, 58-63.
5. **Christensen R.M. 2013.** Theory of Viscoelasticity. Dover Publications, Mineola, New York.
6. **Hernández-Jiménez A., Hernández-Santiago J., Macias-García A., Sánchez-González J., 2002.** Relaxation modulus in PMMA and PTFE fitting by fractional Maxwell model. Polymer Testing, Vol. 21, 325–331.
7. **Heymans N., Bauwens J.C. 1994.** Fractal rheological models and fractional differential equations for viscoelastic behavior. Rheol. Acta, Vol. 33, 210-219.
8. **Kaczorek T., Rogowski K. 2014.** Fractional Linear Systems and Electrical Circuits. Printing House of Bialystok University of Technology, Białystok.
9. **Machado J., Tenreiro V.K., Mainardi F. 2011.** Recent history of fractional calculus. Commun. Nonlinear Sci. Numer. Simul. Communications in Nonlinear Science and Numerical Simulation, Vol. 16, No. 3, 1140–1153.
10. **Mainardi F., Spada G. 2011.** Creep, relaxation and viscosity properties for basic fractional models in rheology. The European Physical Journal Special Topics. Vol. 193, No. 1, 133-160.
11. **Rao M.A. 2014.** Rheology of Fluid, Semisolid, and Solid Foods. Principles and Applications. Springer Science & Business Media, New York.
12. **Schiessel H., Metzler R, Blumen A., Nonnejunacher T.F. 1995.** Generalized viscoelastic models: their fractional equations with solutions. J. Phys. A: Math. Gen. Vol. 28, 6567-6584.
13. **Scott Blair G.W. 1972.** Rheology of foodstuffs, lecture to the technical university in Budapest. Periodica Polytechnica Chemical Engineering, Vol. 16, No. 1, 81-84.
14. **Shapovalov Yu., Mandziy B., Bachyk D. 2013.** Optimization of linear parametric circuits in the frequency domain. ECONTECHMOD, Vol. 2, No. 4, 73-77.
15. **Stankiewicz A. 2007.** Identification of the relaxation spectrum of viscoelastic plant materials. PhD Thesis, Agriculture University of Lublin, Lublin.
16. **Stankiewicz A. 2012.** Algorithm of relaxation modulus identification using stress measurements from the real test of relaxation. Inżynieria Rolnicza, Vol. 4(139), 389-400.
17. **Stankiewicz A. 2012.** On measurement point-independent identification of Maxwell model of viscoelastic materials. TEKA Commission of Motorization and Energetics in Agriculture, Vol. 12, No. 22, 223-229.
18. **Stankiewicz A. 2013.** Selected methods and algorithms for the identification of models used in the rheology of biological materials. Tow. Wyd. Nauk. Libropolis, Lublin.
19. **Stankiewicz A. 2018.** Fractional Maxwell model of viscoelastic biological materials. Proc. Contemporary Research Trends in Agricultural Engineering, BIO Web Conf. Vol. 10, 2018, Article No. 02032, Pages: 8, DOI: https://doi.org/10.1051/bioconf/20181002032.
20. **Starek A., Kusińska E. 2016.** The variability of mechanical properties of the kohlrabi stalk parenchyma. ECONTECHMOD, Vol. 5. No. 3, 9-18.

21. **Wagner C.E., Barbati A.C., Engmann J., Burbidge A.S., McKinley G.H. 2017.** Quantifying the consistency and rheology of liquid foods using fractional calculus. Food Hydrocolloids Vol. 69, 242-254.
22. **Wcisło G. 2017.** Determining the effect of the addition of bio-components AME on the rheological properties of biofuels. ECONTECHMOD, Vol. 6, No. 1, 105–110.